in PhCN but $(OEP)Si(CH_3)_2$ is oxidized at slightly more negative potentials (see Figure 4d). $(OEP)Si(CH_3)_2$ can also be oxidized by four electrons in the potential range of PhCN. The single reversible reduction is diffusion-controlled and occurs at $E_{1/2}$ = −1.46 V. Spectroelectrochemical monitoring of this reaction indicates that the initial product is a porphyrin π anion radical, $[(OEP)Si(CH_3)_2]^-$. These spectral data are given in Table V.

In summary, the oxidative and reductive behaviors of $(OEP)Si(R)_2$ are basically identical for R = CH_3 and C_6H_5. Combining these data with the electrochemistry of $(OEP)Si(C_6H_5)OH$ enables one to derive an overall electrochemical mechanism for all of these complexes. This mechanism is shown in Scheme III for R = C_6H_5.

Comparisons between $(OEP)Si(R)_2$ and $(OEP)Ge(R)_2$. The physicochemical properties of neutral $(OEP)Si(R)_2$ porphyrins are similar to those of $(OEP)Ge(R)_2$.[10] The ^1H NMR, IR, and UV–visible spectroscopies as well as the electrochemical data show this unambiguously.

$(OEP)M(R)ClO_4$ (M = Si or Ge) complexes are oxidized between +1.40 and +1.47 V while the first electrochemical oxidation of $(OEP)M(R)_2$ occurs between +0.72 and +0.88 V. The first oxidation product of $(OEP)M(R)ClO_4$ gives a π cation radical. In contrast, the final product of $(OEP)M(R)_2$ oxidation is not a cation radical due to the rapid cleavage of one metal–carbon bond that occurs after the initial electrochemical oxidation. This instability of the dialkyl and diaryl complexes is related to the site of electron abstraction. The orbital involved in this process could be a σ molecular orbital, i.e., an orbital of the axial ligand that overlaps an orbital of the metal rather than a π ring orbital.

Acknowledgment. The support of the National Science Foundation (Grants No. CHE-8515411 and No. INT-8413696) and the CNRS is gratefully acknowledged.

Registry No. $(OEP)Si(CH_3)_2$, 112896-49-8; $(OEP)Si(C_6H_5)_2$, 112896-50-1; $(OEP)Si(C_6H_5)OH$, 112896-51-2; $(OEP)Si(OH)_2$, 50820-15-0.

Contribution from the Department of Chemistry, University of Houston, Houston, Texas 77004, Laboratoire de Chimie-Physique Générale, Faculté des Sciences de Rabat, Université Mohammed V, Rabat, Morocco, and Laboratoire de Synthèse et d'Electrosynthèse Organometallique, Associé au CNRS (UA 33), Faculté des Sciences "Gabriel", Université de Dijon, 21100 Dijon, France

Electrochemical and Spectroelectrochemical Studies of Nickel(II) Porphyrins in Dimethylformamide

K. M. Kadish,*[1a] D. Sazou,[1a] Y. M. Liu,[1a] A. Saoiabi,[1b] M. Ferhat,[1b] and R. Guilard*[1c]

Received July 8, 1987

The electrochemistry of $(P)Ni^{II}$ in DMF is reported where P is the dianion of tetrapyridylporphyrin (TpyP), tetrakis(*p*-(sodiosulfonato)phenyl)porphyrin (T(*p*-SO_3Na)PP), and tetrakis(*p*-diethylaminophenyl)porphyrin (T(*p*-Et_2N)PP). Each electrode reaction was monitored by cyclic voltammetry, rotating-disk voltammetry, spectroelectrochemistry, and ESR spectroscopy, and on the basis of these data, an overall oxidation–reduction mechanism for each complex is presented. All three compounds can be reduced by one electron to form π anion radicals or oxidized by one or two electrons to form π cation radicals and dications. Additional oxidations are also associated with the diethylamino groups on (T(*p*-Et_2N)PP)Ni. Reduced (T(*p*-SO_3Na)PP)Ni and (T(*p*-Et_2N)PP)Ni are stable, but (TpyP)Ni undergoes demetalation after reduction by two electrons at the porphyrin π ring system. This is the first example for demetalation of an electroreduced nickel porphyrin and contrasts with results for other nickel porphyrins, which are quite stable after electroreduction. The effect of porphyrin ring structure on the electrochemical behavior of each complex is discussed and compared with that of other related metalloporphyrins.

Introduction

The electrochemical reactions of synthetic nickel porphyrins have been characterized in various nonaqueous solvent/supporting electrolyte combinations, and numerous details regarding redox potentials and the site of electron transfer have been presented.[2-9] Studies of nickel porphyrins are of interest with respect to their biological relevance[10-12] and to the fact that they are found in shale oils.[13] In this regard, nickel and vanadyl porphyrins are the main organic geochemical constituents in fossil plant material.[14,15]

The spectroscopic and physical properties of several tetrapyridylporphyrins and tetrakis(*p*-sulfonatophenyl)porphyrins have been investigated.[6,16-22] In the present study we report the electrochemistry and spectroelectrochemistry of (TpyP)Ni, (T(*p*-SO_3Na)PP)Ni, and (T(*p*-Et_2N)PP)Ni in DMF. Structures of these three nickel complexes are shown in Figure 1.

The electrochemistry of (TpyP)Ni and (T(*p*-SO_3Na)PP)Ni has not been reported in the literature, but that of (T(*p*-Et_2N)PP)Ni in CH_2Cl_2 is known.[2] This compound undergoes one reduction and either two or three oxidations depending upon the solvent and supporting electrolyte system. The complex is oxidized at $E_{1/2}$ = 0.63 and 1.11 V and reduced at −1.36 V in CH_2Cl_2 when TBAP is used as the supporting electrolyte.[2] A third oxidation of (T(*p*-Et_2N)PP)Ni is also observed at $E_{1/2}$ = 1.4 V when $TBA(PF_6)$ is used as the supporting electrolyte. Identical reductive behavior is observed in CH_2Cl_2 and DMF, but the oxidative properties are quite different in these two solvents containing 0.1 M TBAP. Mechanisms for reduction and oxidation of the three complexes

(1) (a) University of Houston. (b) Université Mohammed V. (c) Université de Dijon.
(2) Chang, D.; Malinski, T.; Ulman, A.; Kadish, K. M. *Inorg. Chem.* **1984**, *23*, 817.
(3) Wolberg, A.; Manassen, J. *Inorg. Chem.* **1970**, *9*, 2365.
(4) Wolberg, A.; Manassen, J. *J. Am. Chem. Soc.* **1970**, *92*, 2982.
(5) Dolphin, D.; Niem, T.; Felton, R. H.; Fajita, S. *J. Am. Chem. Soc.* **1975**, *97*, 5288.
(6) Johnson, E. E.; Niem, T.; Dolphin, D. *Can. J. Chem.* **1978**, *56*, 1381.
(7) Kadish, K. M.; Morrison, M. M. *Inorg. Chem.* **1976**, *15*, 980.
(8) Felton, R. H.; Linschitz, H. *J. Am. Chem. Soc.* **1966**, *88*, 1113.
(9) Kadish, K. M.; Morrison, M. M. *Bioinorg. Chem.* **1977**, *7*, 107.
(10) Ellefson, W. L.; Whitman, W. B.; Wolfe, R. S. *Proc. Natl. Acad. Sci. U.S.A.* **1982**, *79*, 3707.
(11) Livingston, D. A.; Pfaltz, A.; Schreiber, J.; Eschenmoser, A.; Ankel-Fuchs, D.; Moll, J.; Jaenchen, R.; Thauer, R. K. *Helv. Chim. Acta* **1984**, *67*, 334.
(12) Pfaltz, A.; Livingston, D. A.; Jaun, B.; Diekert, G.; Thauer, R. K.; Eschenmoser, A. *Helv. Chim. Acta* **1985**, *68*, 1338.
(13) Saoiabi, A.; Ferhat, M.; Barbe, J.-M.; Guilard, R. *Fuel* **1983**, *62*, 963.
(14) Baker, E. W.; Palmer, S. E. In *The Porphyrins*; Dolphin, D., Ed.; Academic: New York, 1978; Vol. 1A, Chapter 11, p 485.
(15) Dickson, F. E.; Petrakis, L. *J. Phys. Chem.* **1970**, *74*, 2850.
(16) Neri, B. P.; Wilson, G. S. *Anal. Chem.* **1973**, *45*, 442.
(17) Williams, R. F. X.; Hambright, P. *Bioinorg. Chem.* **1978**, *9*, 537.
(18) Pasternack, R. F. *Ann. N.Y. Acad. Sci.* **1973**, *206*, 614.
(19) Pasternack, R. F.; Francesconi, L.; Raff, D.; Spiro, E. *Inorg. Chem.* **1973**, *12*, 2606.
(20) Kalyanasundaram, K. *Inorg. Chem.* **1984**, *23*, 2453.
(21) Brookfield, R. L.; Ellul, H.; Harriman, A. *J. Photochem.* **1985**, *31*, 97.
(22) Barley, M. H.; Rhodes, M. R.; Meyer, T. J. *Inorg. Chem.* **1987**, *26*, 1746.

0020-1669/88/1327-1198$01.50/0

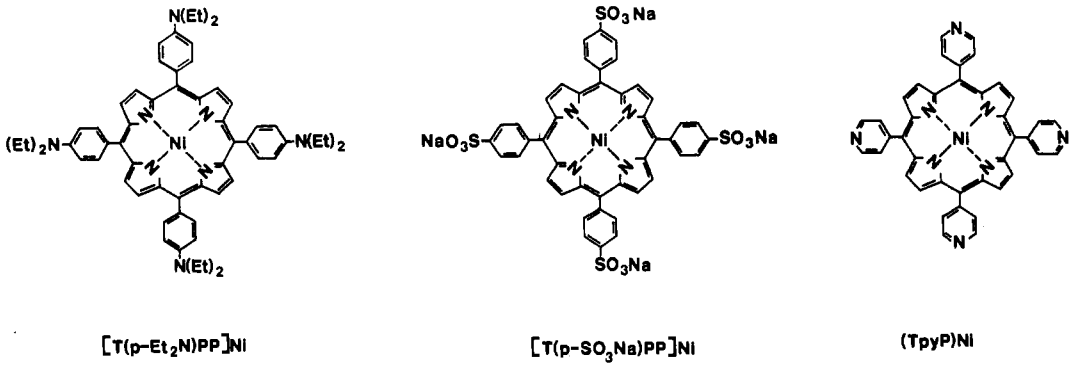

Figure 1. Structures of investigated nickel(II) porphyrins.

in Figure 1 also differ from each other as well as from mechanisms for oxidation or reduction of other nickel(II) porphyrins previously described in the literature.

Experimental Section

Instrumentation and Methods. Cyclic voltammetric and polarographic measurements were carried out on a BAS 100 electrochemical analyzer or an EG&G Princeton Applied Research Model 174A polarographic analyzer. Current–potential curves were recorded with a Houston 9002A X-Y recorder for potential sweep rates less than 0.5 V/s. Platinum rotating-disk voltammograms were obtained with an IBM Instruments Model 225 voltammetric analyzer. A conventional three-electrode system was used. This consisted of a Pt-button working electrode, a Pt-wire counter electrode and an aqueous saturated KCl calomel electrode (SCE) as the reference electrode. This electrode was separated from the working electrode compartment by a glass diaphragm.

Electronic absorption spectra of the neutral metalloporphyrins were obtained with an IBM 9430 UV–visible spectrophotometer using quartz cells with 1.0-cm path lengths. Spectroelectrochemical measurements were performed with a Tracor-Northern 1710 optical spectrometer/multichannel analyzer coupled with a TN-1710-24 floppy disk system for spectral acquisitions. Time-resolved spectra were obtained by using a vacuum-tight, short path length thin-layer spectroelectrochemical cell with a doublet platinum-gauze working electrode.[23]

ESR spectra at liquid-nitrogen temperatures were recorded on an IBM Model ER 100D spectrometer, equipped with an ER 040-X microwave bridge and an ER 080 power supply. The cavity was cooled by a stream of liquid nitrogen that was constantly passed through the variable-temperature insert. The samples were introduced into the cavity in a sealed quartz tube immersed in a liquid-nitrogen Dewar. The g values were measured relative to that of diphenylpicrylhydrazyl (DPPH) ($g = 2.0036 \pm 0.0003$).

Reagents. The supporting electrolyte was tetra-*n*-butylammonium perchlorate (TBAP), which was purchased from Eastman Chemicals, recrystallized from ethyl alcohol, and dried in vacuo prior to use. The concentration of TBAP was 0.2 M for bulk electrolysis and spectroelectrochemical measurements and 0.1 M for the polarographic and voltammetric measurements. *N,N*-Dimethylformamide (DMF) was obtained from Eastman Chemicals and was twice vacuum distilled over molecular sieves prior to use.

All solvent/supporting electrolyte solutions were deaerated with purified nitrogen before the solid porphyrin was added to solution. A nitrogen stream was also passed above the solution during measurements. All electrochemical experiments were performed at a constant temperature of 23 ± 0.1 °C except where otherwise stated. ESR spectra were obtained at liquid-nitrogen temperatures.

Synthesis of the investigated porphyrins is described below.

(TpyP)Ni. Free base $(TpyP)H_2$ was prepared according to the method of Longo et al.[24] but with some modification to the experimental procedure. In the present preparation 18.2 mL of pyrrole and 25 mL of pyridine 2-carboxaldehyde were added to 1.0 L of propionic acid. Addition of the two last reactants was made drop by drop with stirring, after which the mixture was refluxed for 1 h. This solution was left overnight at room temperature and the solvent evaporated to a final volume of about 30 mL, after which 1.8 L of methanol was added. A crystalline product was obtained after filtration. The crystals were washed with methanol until the solution was transparent and then dried in vacuo. The yield was about 18%. A 2-g sample of $(TpyP)H_2$ and 3.84 g of $NiCl_2 \cdot 6H_2O$ were then refluxed in 400 mL of benzonitrile for 3 h. The obtained porphyrin was filtered, washed with hexane, and dried in vacuo. UV–visible data of (TpyP)Ni in methanol (λ_{max}, nm (ϵ)): 406 (27.2×10^3), 523 (5.0×10^3), and 552 (2.4×10^3).

(T(*p*-SO_3Na)PP)Ni. $(T(p\text{-}SO_3NH_4)PP)H_2$ was prepared by using a modification of Fleischer's method.[25] A 2-g sample of $(TPP)H_2$ and 50 mL of H_2SO_4 were stirred for 8 h at 100 °C. The solution was left overnight at room temperature, filtered, and washed with a small quantity of water after which 300 mL of hot water was added. Neutralization of the pH 9 solution was achieved by addition of ammonia. The solution was evaporated and 75 mL of ammonia with 900 mL of ethanol were added under continuous stirring. The mixture was left for 3 h, dissolved in ethanol, and filtered. $(T(p\text{-}SO_3NH_4)PP)H_2$ was obtained after evaporation of the solution. The free base was then washed with hexane and dried for 4 h in vacuo. The yield was about 95%. A 3.5-g sample of $(T(p\text{-}SO_3NH_4)PP)H_2$ and 4.16 g of $NiCl_2 \cdot 6H_2O$ were then refluxed in 600 mL of DMF for 2 h under a nitrogen atmosphere. Metalation was confirmed by UV–visible spectroscopy. The solvent was removed and the porphyrin chromatographed on an alumina column using water–methanol and acetone. The chromatographed solution was evaporated and the porphyrin dissolved in ethanol. After removal of insoluble components (alumina and other impurities), the solvent was evaporated. The resulting solid compound was washed with hexane and dried in vacuo. UV–visible data of $(T(p\text{-}SO_3NH_4)PP)Ni$ in water (λ_{max}, nm (ϵ)): 406 (183×10^3), 521 (12.5×10^3). This complex was converted to $(T(p\text{-}SO_3Na)PP)Ni$ by passage through a column of Amberlite CG 120, 100-200 mesh, sodium form.

(T(*p*-Et_2N)PP)Ni. The synthesis of $(T(p\text{-}Et_2N)PP)H_2$ was carried out by using a modified method of Datta-Gupta et al.[26] In the utilized method, 25 g of $Et_2NC_6H_4CHO$ were refluxed while 10 mL of pyrrole was added drop by drop. A viscous mixture was obtained after continuous stirring and warming for 5 days. The solution was then cooled to room temperature, and 30 mL of CH_2Cl_2 was added. The solution was warmed for 30 min and after cooling, 500 mL of acetone were added. The crystals obtained were filtered, washed with acetone and dried in vacuo for 4 h. The yield was about 14%. A 1-g sample of $(T(p\text{-}Et_2N)PP)H_2$ and 1.41 g of $NiCl_2 \cdot 6H_2O$ were then refluxed in 500 mL of DMF under a continuous nitrogen stream for 8 h. After evaporation of the solvent, the solid product was dissolved in CH_2Cl_2, washed with water, and dried by $MgSO_4$. The crystals obtained after evaporation were washed with hexane and dried in vacuo. The yield was about 98%. UV–visible data for $(T(p\text{-}Et_2N)PP)Ni$ in CH_2Cl_2 (λ_{max}, nm (ϵ)): 432 (113×10^3), 533 (16.2×10^3), 574 (8.1×10^3).

Results and Discussion

Electrochemistry of (TpyP)Ni. Figure 2 illustrates rotating-disk voltammograms for the reduction of (TpyP)Ni (solid line) and $(TpyP)H_2$ (dashed line) in DMF containing 0.1 M TBAP. (TpyP)Ni is reduced in three steps, which occur at $E_{1/2} = -0.45$, -1.08, and -1.35 V. These processes are labeled as reactions I, II, and III. Free base $(TpyP)H_2$ is reduced in two steps, which occur at $E_{1/2} = -0.86$ and -1.4 V. These latter potentials are in good agreement with $E_{1/2}$ values (measured vs Ag/Ag^+) for reduction of $(TpyP)H_2$ in DMF.[17]

The first two reductions of $(TpyP)H_2$ and (TpyP)Ni can be assigned as involving a stepwise one-electron addition to the porphyrin π ring system. The third reduction of (TpyP)Ni at $E_{1/2}$

(23) Lin, X. Q.; Kadish, K. M. *Anal. Chem.* **1985**, *57*, 1498.
(24) Longo, F. R.; Finarelli, M. G.; Kin, J. B. *J. Heterocycl. Chem.* **1969**, *6*, 927.
(25) Fleischer, E. B.; Palmer, J. M.; Srivastava, T. S.; Chatterjee, A. *J. Am. Chem. Soc.* **1971**, *93*, 3162.
(26) Datta-Gupta, N.; Bardos, T. *J. Heterocycl. Chem.* **1966**, *3*, 495.

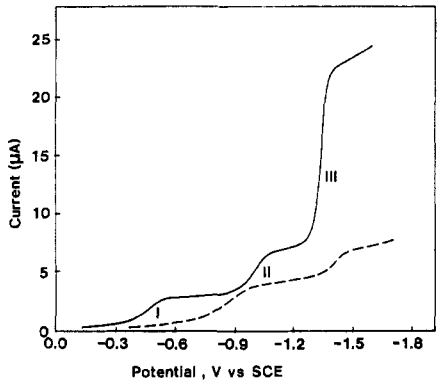

Figure 2. Rotating-disk voltammograms illustrating the reduction of 1.25 × 10^{-3} M (TpyP)Ni (—) and 1.30 × 10^{-3} M (TpyP)H_2 (--) in DMF containing 0.1 M TBAP. Scan rate = 0.01 V/s. Rotation rate = 400 rpm.

= −1.35 V (reaction III, Figure 2) involves a multielectron transfer and occurs at virtually the same potential as for reduction of Ni^{2+} under the same experimental conditions.[27] This suggests that a demetalation of the complex has occurred after generation of the $[(TpyP)Ni]^{2-}$ dianion and that the liberated Ni(II) (which should form $Ni(ClO_4)_2$ in 0.1 M TBAP) is reduced to Ni(0) via a two-electron-transfer step in wave III.

The potential separations $|E_p - E_{p/2}|$ and $|E_{pc} - E_{pa}|$ for the first reduction of (TpyP)Ni by cyclic voltammetry (process I, Figure 3a) are close to 60 mV at low sweep rates and increase to about 100 mV at higher potential scan rates ($v > 0.1$ V/s). The second reduction of (TpyP)Ni (wave II) is irreversible in that there is no coupled reoxidation peak. The third process is also irreversible as seen by the cyclic voltammogram in Figure 3b.

Controlled-potential electrolysis of (TpyP)Ni at −1.5 V shows the addition of 3.75 ± 0.15 electrons as the surface of the platinum electrode turns black due to the deposition of Ni(0). This electrodeposited nickel could be dissolved in solution by applying a potential of +0.2 V to the electrode. When this occurred, the yellow color of the solution changed to dark green, a characteristic color of most nickel salt solutions. At this point a new reduction and reoxidation wave of Ni^{2+} appeared. This oxidation is illustrated by peak IV in Figure 3b and Figure 3c, the latter of which is for reduction and reoxidation of $Ni(NO_3)_2$ in DMF. As seen in this figure the oxidation of metallic Ni(0) occurs at somewhat more negative potentials in the absence of NO_3^- ions. In this case, the generated product is most likely $Ni(ClO_4)_2$.

The demetalation of (TpyP)Ni does not occur prior to electroreduction. This is evident from the voltammograms in Figures 2 and 3 as well as the UV–visible spectrum of (TpyP)Ni in DMF. The initial solution of unreduced (TpyP)Ni exhibits no UV–visible bands or voltammetric peaks that can be associated with (TpyP)H_2 (see rotating-disk voltammograms in Figure 2). However, metallic nickel is deposited on the electrode surface after exhaustive electrolysis of (TpyP)Ni at potentials negative of −1.4 V, and the resulting UV–visible spectrum of the solution is identical with the one obtained after controlled-potential reduction of (TpyP)H_2 by two electrons.

The above data provide the first example for demetalation of an electroreduced nickel porphyrin and this contrasts with other nickel porphyrins, which are quite stable after electroreduction.[28] The demetalation of (TpyP)Ni seems to be related to the facile formation of a nickel tetrapyridylporphyrin anion radical and dianion rather than to a reduction of the porphyrin central metal ion as is the case for $[(P)Tl^{III}]^+$ and $(P)Ag^{II}$,[29] both of which demetalate after formation of an unstable $[(P)M^I]^-$ complex. After electrogeneration of $[(P)Ag^I]^-$ there is a further one-electron reduction of the demetalated Ag(I) ion to give deposited silver

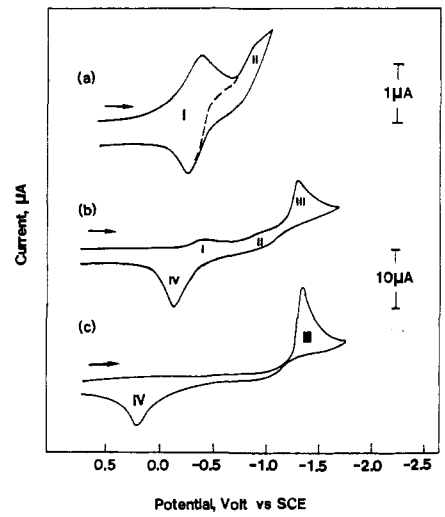

Figure 3. Cyclic voltammograms of (a) 1.38 × 10^{-3} M (TpyP)Ni in DMF containing 0.1 M TBAP between +0.6 and −1.0 V, (b) the same solution but with a scan range between +0.6 and −1.7 V; and (c) 1.55 × 10^{-3} M $Ni(NO_3)_2$ in DMF containing 0.1 M TBAP, at a scan rate of 0.2 V/s.

on the electrode surface and the corresponding free base porphyrin. The electrochemistry of (TpyP)Ni is also different from that of $(P)Ag^{II}$ and $[(P)Tl^{III}]^+$ in that the first two reductions of the nickel complex occur at the porphyrin π ring system and precede demetalation. However, this mechanistic sequence for (TpyP)Ni is similar to that of (TPP)Mo(O), which undergoes demetalation after a two-step reduction at the porphyrin π ring system.[30]

In summary, the first two reductions of (TpyP)Ni in DMF involve addition of electrons to the porphyrin π ring system (processes I and II) while the electrochemical steps III and IV involve a reduction and reoxidation of the liberated Ni^{2+} ion. This sequence of steps is shown in Scheme I.

Scheme I

$$(TpyP)Ni + e^- \xrightarrow{I} [(TpyP)Ni]^-$$

$$[(TpyP)Ni]^- + e^- \underset{}{\overset{II}{\rightleftharpoons}} [(TpyP)Ni]^{2-}$$

$$[(TpyP)Ni]^{2-} \xrightarrow{2H^+} Ni^{2+} + [(TpyP)H_2]^{2-}$$

$$Ni^{2+} + 2e^- \underset{IV}{\overset{III}{\rightleftharpoons}} Ni(0)$$

The fact that the relative current heights of waves I, II, and III in Figure 2 are 1:1:4.7 and not 1:1:2, which is expected for a two-electron reduction of Ni^{2+} to Ni^0, can be attributed to a catalytic reduction of protons from the trace water that remains in DMF even after purification.

Attempts to evaluate the mechanism of $[(TpyP)Ni]^{2-}$ demetalation were carried out by using variable scan rate and low-temperature cyclic voltammetry. These data are shown in Figures 4 and 5. The value of $E_{p/2}$ for reaction II shifts cathodically with increasing scan rate and a plot of $E_{p/2}$ vs log v is linear with a slope of about −30 mV. These data are consistent with the occurrence of a chemical reaction following a diffusion-controlled one-electron transfer (an EC type mechanism)[32,33] and the overall reduction processes shown in Scheme I.

Figure 5 shows cyclic voltammograms of (TpyP)Ni at temperatures between +46 and −62 °C. As the temperature is lowered from 46 °C the currents for all three reductions decrease in intensity while the peak potentials shift in a negative direction.

(27) Gaur, J. N.; Goswami, N. K. *Electrochim. Acta* **1966**, *11*, 939.
(28) Kadish, K. M. *Prog. Inorg. Chem.* **1987**, *34*, 435–605.
(29) Giraudeau, A.; Louati, A.; Callot, H. J.; Gross, M. *Inorg. Chem.* **1981**, *20*, 769.
(30) Malinski, T.; Hanley, P. M.; Kadish, K. M. *Inorg. Chem.* **1986**, *25*, 3229.
(31) Levich, V. G. *Acta Physicochim. URSS* **1942**, *17*, 1257.
(32) Nicholson, R. S.; Shain, I. *Anal. Chem.* **1965**, *37*, 178, 190.
(33) Polcyn, D. S.; Shain, I. *Anal. Chem.* **1966**, *38*, 370; **1968**, *38*, 376.

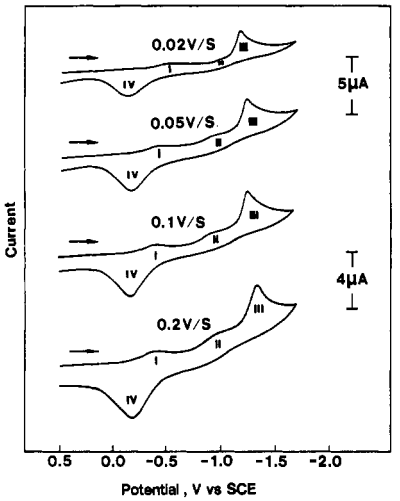

Figure 4. Cyclic voltammograms of 6.3×10^{-4} M (TpyP)Ni at different scan rates in DMF containing 0.1 M TBAP.

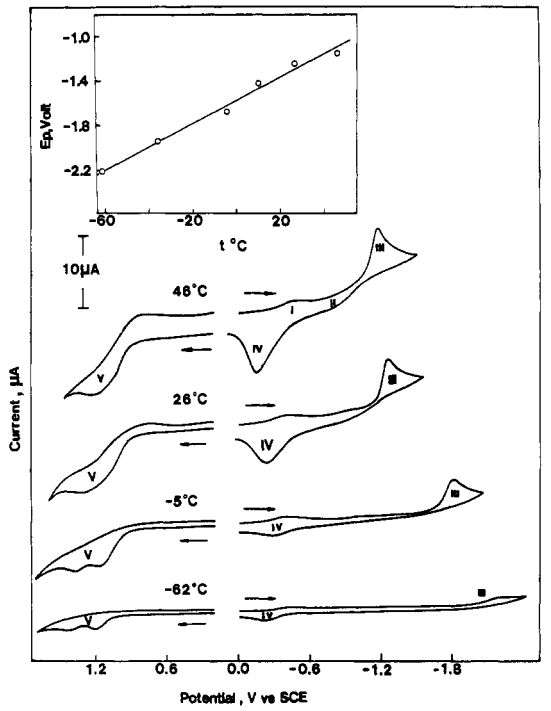

Figure 5. Temperature dependence on the cyclic voltammograms of 1.38×10^{-3} M (TpyP)Ni in DMF containing 0.1 M TBAP. Scan rate = 0.1 V/s. The insert illustrates the linear plot of E_p vs. temperature for reaction III.

The shift of E_p for reaction III as a function of temperature is plotted in the insert of Figure 5. The temperature coefficient of the peak potential is about 9.4 mV/deg and this agrees with a value of 9.9 mV/deg for reduction of $Ni(NO_3)_2$ in DMF under the same experimental conditions.

A demetalation of (TpyP)Ni seems to occur at all temperatures. However, the decrease in peak current for process III with lowering of the temperature was greater for solutions of (TpyP)Ni than $Ni(NO_3)_2$ and can be explained by the fact that the lower temperatures decrease the diffusion coefficients as well as slow down the rate of $[(TpyP)Ni]^{2-}$ demetalation.

The oxidation of (TpyP)Ni is irreversible at all temperatures and has characteristics of a kinetic-controlled process. A single broad wave occurs at temperatures above 25 °C but there are two oxidation waves at low temperatures. This is shown in Figure 5. Controlled potential oxidation of (TpyP)Ni at 1.5 V gave a coulometric value of $n = 2$.

The cyclic voltammograms in Figure 5 indicate the occurrence of one or more EC mechanisms during oxidation of (TpyP)Ni at

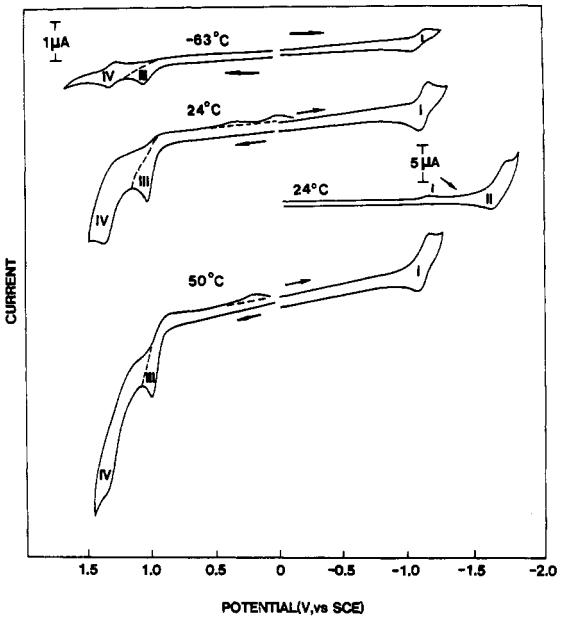

Figure 6. Cyclic voltammograms of 7.55×10^{-4} M [T(*p*-SO_3Na)PP]Ni at three different temperatures in DMF containing 0.1 M TBAP. Scan rate = 0.2 V/s.

temperatures below −5 °C. No ESR signals were obtained after controlled-potential oxidation by two electrons at 1.5 V, and this is consistent with the formation of either $[(TpyP)Ni^{II}]^{2+}$ or $[(TpyP)Ni^{III}]^{2+}$ as the product of electrolysis. However, due to the irreversibility of these processes, a detailed mechanistic evaluation of the oxidations could not be undertaken.

Electrochemistry of (T(*p*-SO_3Na)PP)Ni. The structure of (T(*p*-SO_3Na)PP)Ni is shown in Figure 1. Each of the four SO_3^- groups are associated with a Na^+ ion. The measured conductivity of the complex is 22.04 mho mol^{-1} cm^2 in DMF and can be compared with a molar conductivity of 38.6 mho mol^{-1} cm^2 for TBAP in the same solvent. This implies that (T(*p*-SO_3Na)PP)Ni is not totally dissociated in the solution.

Cyclic voltammograms of (T(*p*-SO_3Na)PP)Ni at three different temperatures are shown in Figure 6. At 24 °C there is a reversible one-electron reduction at $E_{1/2} = -1.20$ V (wave I) and an ill-defined multielectron reduction at $E_{1/2} = -1.70$ V (wave II). The peak potential differences $|E_{pa} - E_{pc}|$ and $|E_p - E_{p/2}|$ for wave I are in the range 60–70 mV and $i_p/v^{1/2}$ = constant, indicating a diffusion-controlled one-electron reversible process. Controlled-potential electrolysis gave a coulometric value of 0.95 electron. The UV–visible spectral changes shown in Figure 7a are not consistent with formation of $[(T(p\text{-}SO_3Na)PP)Ni]^-$ but bulk electrolysis at −1.3 V gives a species with a signal at $g = 2.004$. Thus, the formation of an anion radical is supported by ESR spectra at liquid-nitrogen temperature.

The large currents for wave II may be due to reduction of trace water or to the Na^+ ions associated with the complex. However, this process also contains overlapping currents for reduction of (T(*p*-SO_3Na)PP)Ni. This is shown by spectroelectrochemistry during controlled-potential electrolysis at −1.70 V (Figure 7b). As the electrolysis proceeds, the broad band in the region between 700 and 850 nm increases as the Soret band shifts to 470 nm and decreases in intensity. There are three isosbestic points at 445, 498, and 635 nm. The overall spectral changes recorded during this controlled-potential reduction indicate the presence of the phlorin $[(T(p\text{-}SO_3Na)PP)NiH]^-$, after protonation of $[(T(p\text{-}SO_3Na)PP)Ni]^{2-}$. The protons required for phlorin formation come from the trace water in DMF.

(T(*p*-SO_3Na)PP)Ni is oxidized in two steps, but the reversibility of the reactions depends upon the temperature. At room temperature there are two irreversible oxidations located at $E_p = 0.95$ (wave III) and 1.35 V (wave IV). The peak currents for reaction III are proportional to $v^{1/2}$ as well as to the bulk concentration, thus suggesting a diffusion-controlled process.

Table I. Absorption Maxima and Molar Absorptivities of Nickel Porphyrins in DMF

porphyrin rings	reacn	λ, nm (ε × 10^{-3}, cm^{-1} M^{-1})			
TPP	neutral	415 (17.1)	527 (1.24)		
	redn 1	422 (10.5)	522 (0.96)	647 (0.80)	833 (5.95)
	redn 2	466 (2.50)	524 (1.60)	638 (2.20)	
TpyP	neutral	410 (18.2)	527 (1.50)		
	redn 1	430 (5.01)	810 (4.97)		
	oxidn 1	450 (8.04)	>724 (2.14)		
T(*p*-SO_3Na)PP	neutral	411 (107)	526 (8.86)		
	redn 1	475 (92.5)	522 (9.74)		
	redn 2	450 (48.7)	770 (19.5)		
	oxidn 1	420 (41.9)	432 (41.9)	775 (7.79)	855 (11.7)
	oxidn 2	415 (11.68)			
T(*p*-Et_2N)PP	neutral	446 (121)	540 (14.0)	588 (13.2)	
	redn 1	436 (121)	524 (10.6)		
	redn 2	470 (38.4)	525 (12.8)	630 (3.19)	830 (22.4)
	oxidn 1	507 (61.1)	>730 (31.0)		
	oxidn 2	425 (102)	552 (16.0)		

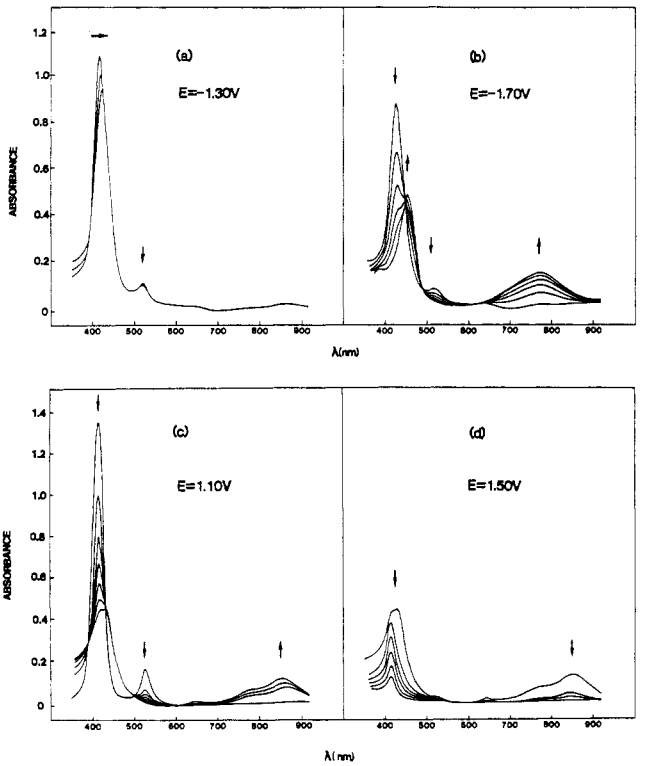

Figure 7. Time-resolved electronic absorption spectra of 3.6 × 10^{-4} M [T(*p*-SO_3Na)PP]Ni during controlled-potential electrolysis in DMF containing 0.2 M TBAP at (a) −1.30, (b) −1.70, (c) +1.10, and (d) +1.5 V.

Reaction IV involves the coulometric abstraction of more than two electrons at room temperature. The irreversibility of wave III supports the existence of a chemical reaction that follows process III and leads to a product which is further oxidized in process IV. At low temperatures, the chemical reaction is slowed down. Under these conditions process IV becomes reversible and involves the overall abstraction of two electrons (see voltammograms at −63 °C in Figure 6). Finally the appearance of a reduction wave at about 0.3 V (Figure 6) suggests that protons are produced during the second oxidation of (T(*p*-SO_3Na)PP)Ni. This reaction occurs at the edge of the solvent and probably involves an oxidation of the DMF.

Spectra obtained during controlled-potential oxidation of (T(*p*-SO_3Na)PP)Ni at 1.1 V are shown in Figure 7c,d. There are four isosbestic points at 395, 435, 500, and 600 nm. The original absorption peaks at 411 and 526 nm decrease in intensity during this oxidation while a band at 800–900 nm increases, thus indicating formation of a π-cation radical. When the controlled potential is set to +1.50 V, the band at 800–900 nm decreases and finally disappears. These latter set of spectra are shown in Figure 7d, and spectral data for all of the products are given in Table I.

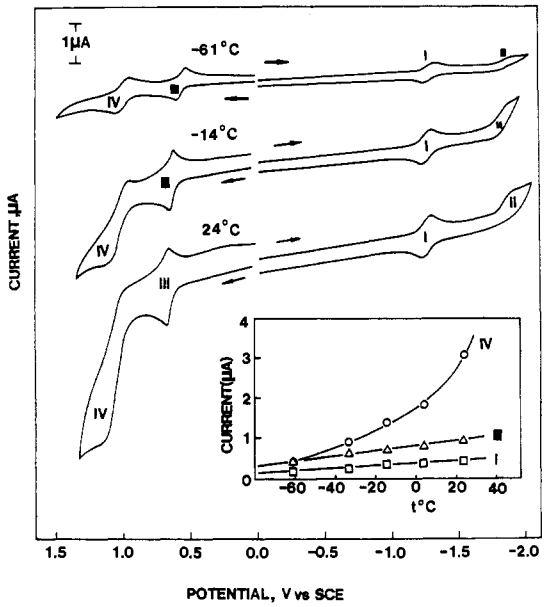

Figure 8. Cyclic voltammograms of 8.06 × 10^{-4} M [T(*p*-Et_2N)PP]Ni at different temperatures in DMF containing 0.1 M TBAP. Scan rate = 0.1 V/s. The insert illustrates the temperature dependence of the oxidation currents for processes I, III, and IV.

Electrochemistry of (T(*p*-Et_2N)PP)Ni. Cyclic voltammograms of (T(*p*-Et_2N)PP)Ni at different temperatures in DMF are shown in Figure 8. The room-temperature voltammogram shows a reversible reduction at $E_{1/2}$ = −1.27 V and an irreversible reduction at E_p = −1.90 V. There is also a two-electron oxidation at $E_{1/2}$ = 0.68 V and another irreversible multielectron oxidation at E_p = 1.10 V. Both the first reduction and the first oxidation are diffusion controlled as indicated by the linearity of i_p with $v^{1/2}$.

The electrochemistry of (T(*p*-Et_2N)PP)Ni in DMF is different from that reported in CH_2Cl_2 where voltammograms are characterized by two or three well-defined room-temperature oxidation waves depending upon the supporting electrolyte.[2] The reduction of (T(*p*-Et_2N)PP)Ni occurs at slightly more negative potentials in CH_2Cl_2 ($E_{1/2}$ = −1.36 V)[2] than in DMF ($E_{1/2}$ = −1.27 V), and this can be attributed to the different coordinating abilities of the solvents. DMF is a strongly coordinating solvent while CH_2Cl_2 is a poorly coordinating one.[34,35]

The peak shape $|E_p - E_{p/2}|$ is about 60 mV for the first reduction of (T(*p*-Et_2N)PP)Ni at room temperature (process I, Figure 8)

(34) Kolthoff, I. M.; Lingane, J. J. In *Polarography*, 2nd ed.; Interscience: New York, 1952.
(35) Sawyer, D. T.; Roberts, J. L. In *Experimental Electrochemistry for Chemists*; Wiley: New York, 1975.

Table II. Half-Wave Potentials, $E_{1/2}$, and Number of Electrons, n, for Oxidation and Reduction of (P)Ni Complexes in DMF

porphyrin macrocycle, P	$E_{1/2}$, V vs SCE (n)					
	redn				oxidn	
	1st	2nd	3rd	4th	1st	2nd
TPP	−1.17 (1)	−1.75 (1)				
TMpyP[a]	−0.50 (2)	−0.62 (1)	−0.82 (2)	−1.01 (1)		
TpyP	−0.45 (1)	−1.08 (1)	−1.35[b]		1.10 (2)	
T(p-SO_3Na)PP	−1.20 (1)	−1.70			0.92 (2)	1.40
T(p-Et_2N)PP	−1.27 (1)	−1.90			0.68 (2)	1.10

[a] Kadish, K. M.; Sazou, D.; Liu, Y. M.; Saoiabi, A.; Ferhat, M.; Guilard, R. *Inorg. Chem.* **1988**, *27*, 686. [b] Reaction corresponds to the reduction of liberated Ni^{2+} after demetalation of (TpyP)Ni (see text).

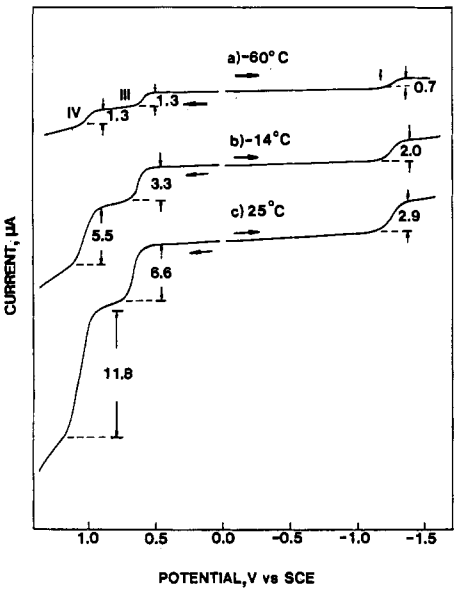

Figure 9. Platinum rotating-disk voltammograms of 8.06×10^{-4} M [T(p-Et_2N)PP]Ni at different temperatures in DMF containing 0.1 M TBAP. Scan rate = 0.01 V/s. Rotation rate = 1000 rpm.

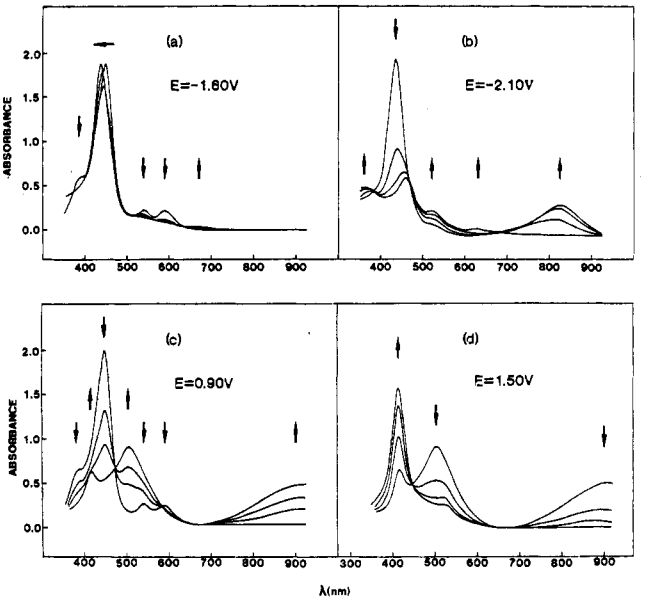

Figure 10. Time-resolved electronic absorption spectra of 2.96×10^{-4} M [T(p-Et_2N)PP]Ni in DMF containing 0.2 M TBAP, during controlled-potential electrolysis at (a) −1.6, (b) −2.1, (c) +0.9, and (d) +1.5 V.

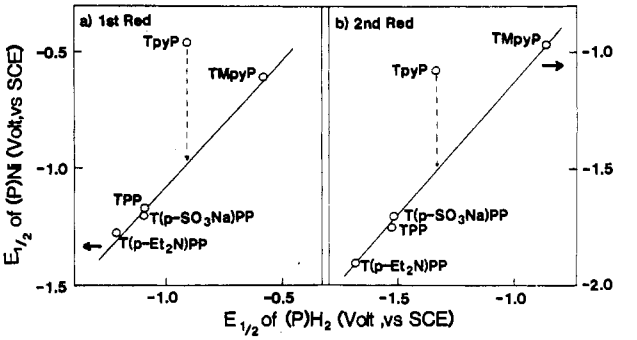

Figure 11. Half-wave potentials measured for (a) the first and (b) the second reduction of various (P)Ni complexes versus half-wave potentials for the first and second reductions of the corresponding $(P)H_2$ free base in DMF containing 0.1 M TBAP.

and about 35 mV for oxidation process III under the same conditions. This suggests a reversible one-electron reduction and a reversible two-electron oxidation. Coulometric measurements at room temperature gave 1.1 electrons transferred in the first reduction, but greater than two electrons were coulometrically obtained for the first oxidation.

The variation of peak currents for processes I, III, and IV with temperature are shown in the insert of Figure 8. At −60 °C the oxidation peak III involves a quasi-reversible two-electron-transfer process, and the currents for oxidation peaks III and IV are equal. The same oxidative behavior is observed for tertiary aromatic amines in nonaqueous solutions and the principal oxidation products are monocation radicals that rapidly dimerize with the parent compound to form benzidine derivatives.[36]

Rotating-disk voltammograms of (T(p-Et_2N)PP)Ni at different temperatures are depicted in Figure 9. At 25 °C the ratio of currents for wave IV (11.8 μA) to wave I (2.9 μA) is 4.07, which suggests a four-electron oxidation and a one-electron reduction at room temperature. Also, the current for oxidation wave III is half that of wave IV, indicating a two-electron transfer for process III. However, at −60 °C the currents for peaks III and IV are equal, indicating equal numbers of electrons transferred at this temperature.

The surface of the electrode is substantially contaminated after the second oxidation of (T(p-Et_2N)PP)Ni at room and higher temperatures. This is related to the electrooxidative polymerization of amino-substituted tetraphenylporphyrins, which will form a polyporphyrin film on the electrode surfaces.[37] At low temperatures these polymerization reactions are slowed down. The low temperatures also lead to stabilization of the electrogenerated porphyrin cation radicals, and the second oxidation of (T(p-Et_2N)PP)Ni is then easily observed.

Spectra recorded during controlled-potential reduction and oxidation of neutral (T(p-Et_2N)PP)Ni are shown in Figure 10. The spectral changes in Figure 11a were recorded during controlled-potential reduction at −1.6 V. The final time-resolved spectra do not show characteristic π-anion radical absorbance bands in the 800–900-nm region, but an ESR spectrum at liquid nitrogen temperature gives a signal at $g = 2.003$ for the reduction product and supports assignment of a porphyrin π-anion radical. The absence of absorbance bands between 800 and 900 nm in Figure 10a can be attributed to a subsequent protonation reaction

(36) Seo, E. T.; Nelson, R. F.; Fritsch, J. M.; Marcoux, L. S.; Leedy, D. W.; Adams, R. N. *J. Am. Chem. Soc.* **1966**, *88*, 3498.
(37) Bertelheim, A.; White, B. A.; Raybuck, S. A.; Murray, R. W. *Inorg. Chem.* **1987**, *26*, 1009.

and phlorin formation that slows down or does not occur at low temperatures. A broad absorbance band appears around 820 nm during the second reduction of (T(*p*-Et_2N)PP)Ni while weak bands emerge at 520 and 620 nm (see Figure 10b). This type of spectrum corresponds to a phlorin anion.[16,38]

The spectral changes in Figure 10c were obtained when the applied potential was set at 0.9 V. Both the changes in the Soret band region and the strong absorptions at wavelengths above 750 nm suggest a delocalization of charge over two of the four diethylamino groups. The final oxidation product of (T(*p*-Et_2N)PP)Ni is not ESR active, and the UV-visible spectrum is similar to that obtained after the two-electron oxidation of the same compound in CH_2Cl_2.[2]

Spectra recorded during the second oxidation of (T(*p*-Et_2N)PP)Ni are shown in Figure 10d and indicate a decreased band at 507 nm and an increased absorption band at 446 nm. The absorption bands at wavelengths greater than 750 nm decrease in intensity as all four diethylamino groups are oxidized. A catalytic oxidation of DMF also occurs at room temperature (see cyclic voltammogram at 24 °C in Figure 8) and results in generation of a porphyrin species with a Soret band at 446 nm and no broad bands between 750 and 950 nm.

Effect of the Porphyrin Macrocycle Basicity on Reversible Reduction Potentials. Substituent effect on porphyrin redox reactions have often been expressed by plots of $E_{1/2}$ vs. σ where σ is a measure of the electron-donating or electron-withdrawing substituent on the porphyrin ring.[28] The $E_{1/2}$ for reduction of free-base porphyrins to their radical anions in DMF solutions has been also used as a measure of porphyrin ring electron basicity[17] and is utilized in this present study for evaluating substituent effects.

Figure 11 shows the relationship between $E_{1/2}$ for the first and second reduction of the nickel porphyrins vs $E_{1/2}$ for reduction of the corresponding free base porphyrins in DMF. [T(*p*-Et_2N)PP]H_2 and (TPP)Ni are insoluble in DMF, and values of $E_{1/2}$ were measured in PhCN or in a mixture of benzene and DMF, respectively. The exact conditions and a list of half-wave potentials are given in Table II.

Half-wave potentials for the first reduction of a given nickel(II) porphyrin at the π ring system are generally more negative by 100-200 mV than $E_{1/2}$ for reduction of the corresponding free base porphyrin.[28] However, $E_{1/2}$ for the first reduction of (TpyP)Ni (-0.45 V) is 410 mV less negative than $E_{1/2}$ for the first reduction of (TpyP)H_2 (-0.86 V). The first reduction of (TpyP)Ni is also less negative than $E_{1/2}$ for the first reduction of positively charged [(TMpyP)Ni]$^{4+}$. A positive charge is not present in (TpyP)Ni, but $E_{1/2}$ values are similar to those for reduction of the easily reduced nickel(II) tri- and tetracyano-substituted tetraphenylporphyrins in DMF.[39] For example, the $E_{1/2}$ of -0.45 V is approximately midway between potentials for reduction of (TPP$(CN)_4$)Ni ($E_{1/2}$ = -0.330 V)[39] and (TPP$(CN)_3$)Ni ($E_{1/2}$ = -0.530 V)[39] in the same solvent system. On the basis of this comparison, one might predict that (TpyP)H_2 would also be reduced at an $E_{1/2}$ midway between values for reduction of (TPP$(CN)_4$)H_2 ($E_{1/2}$ = -0.120 V)[40] and (TPP$(CN)_3$)H_2 ($E_{1/2}$ = -0.330 V)[40] or at about -0.22 V. The actual $E_{1/2}$ value is -0.86 V. This latter value of $E_{1/2}$ for reduction of the free base complex is not unexpected, and the difference between the predicted and experimentally observed reduction potentials are thus actually associated with (TpyP)Ni rather than with (TpyP)H_2. This is evident from the data in Figure 11, which show deviations of 520 mV and 390 mV from linear plots involving the first and second reductions of (P)Ni and (P)H_2, respectively.

In summary, it is important to emphasize the unexpected demetalation of (TpyP)Ni after a two-electron reduction at the porphyrin π ring system. The metal ion size and geometry of the complex are not consistent with a demetalation. On the other hand, the unexpected facile reduction of the macrocyclic porphyrin ring is probably related to this demetalation, which leads to the ultimate formation of Ni(0) and a free base porphyrin in solution.

Acknowledgment. The support of the National Science Foundation (Grant No. CHE-8515411 and Grant No. INT-8413696) is gratefully acknowledged.

Registry No. (TPP)Ni, 14172-92-0; [(TPP)Ni]$^-$, 88669-50-5; [(TPP)Ni]$^{2-}$, 112739-99-8; [(TMpyP)Ni]$^{4+}$, 48242-71-3; [(TMpyP)Ni]$^{3+}$, 112739-97-6; [(TMpyP)Ni]$^{2+}$, 112740-00-8; [(TMpyP)Ni]$^+$, 112763-16-3; [(TMpyP)Ni], 112763-17-4; (TpyP)Ni, 14514-68-2; [(TpyP)Ni]$^-$, 112739-98-7; [(TpyP)Ni]$^{2-}$, 112740-01-9; [(TpyP)Ni]$^+$, 112740-04-2; (T(*p*-SO_3Na)PP)Ni, 67204-04-0; [(T(*p*-SO_3Na)PP)Ni]$^-$, 112740-07-5; [(T(*p*-SO_3Na)PP)Ni]$^{2-}$, 112740-02-0; [(T(*p*-SO_3Na)PP)Ni]$^+$, 112740-05-3; [(T(*p*-SO_3Na)PP)Ni]$^{2+}$, 112740-06-4; (T(*p*-Et_2N)PP)Ni, 88669-48-1; [(T(*p*-Et_2N)PP)Ni]$^-$, 88669-57-2; [(T(*p*-Et_2N)PP)Ni]$^{2-}$, 112740-03-1; [(T(*p*-Et_2N)PP)Ni]$^+$, 88669-52-7; [(T(*p*-Et_2N)PP)Ni]$^{2+}$, 88669-62-9; TPyP, 16834-13-2; Ni, 7440-02-0.

(38) Felton, R. H. In *The Porphyrins*; Dolphin, D., Ed.; Academic: New York, 1978; Vol. 5, p 53.

(39) Callot, H. J.; Giraudeau, A.; Gross, M. *J. Chem. Soc., Perkin Trans. 2* **1975**, *12*, 1321.

(40) Giraudeau, A.; Callot, H. J.; Jordan, J.; Ezahr, E.; Gross, M. *J. Am. Chem. Soc.* **1979**, *101*, 3857.

Contribution from the Department of Chemistry, University of Victoria, Victoria, BC, Canada V8W 2Y2

Kinetics and Mechanism of Electron-Transfer Reactions of Bis((-)-(*R*)-2-methyl-1,4,7-triazacyclononane)nickel(II) and -nickel(III) Complexes

A. McAuley* and C. Xu

Received July 23, 1987

A synthesis of the title ligand ((-)-(*R*)-Me-9-aneN_3) is reported together with preparations of the nickel(II) and nickel(III) complexes. There is retention of an NiN_6 chromophore in both oxidation states. The nickel(II) species is very stable in aqueous media with a slow acid-catalyzed hydrolysis (k_H = 1.8 × 10^{-4} M^{-1} s^{-1} at 30 °C). The nickel(III) ion shows only slight decomposition at pH 3 and is indefinitely stable in acetonitrile. Rate constants for a series of outer-sphere electron-transfer reactions have been determined (with $Co(phen)_3^{2+}$ and I^- reducing Ni(III) and with Ni(cyclam)$^{3+}$, Ni(9-aneN_3)$_2^{3+}$, Ni^{IV}(oxime), and Co^{3+}(aq) oxidizing Ni(II)). Use of a Marcus cross-correlation leads to a self-exchange rate for the $NiL_2^{3+/2+}$ couple of (1.2 ± 0.5) × 10^4 M^{-1} s^{-1} (I = 1.0 M). The data are of interest in that there is retention of the octahedral symmetry at the metal center. Possible correlations of rates of electron exchange with bond extension in the inner coordination sphere are discussed.

Introduction

From being in a relatively rare oxidation state a decade ago, nickel(III) has become much more prominent as an accessible form[1-8] not only in polyaza macrocyclic complexes but also in several oligopeptide species[9,10] and biological systems, principally those involving methanogenic bacteria.[11-13] In the latter, there

(1) Gore, E. S.; Busch, D. H. *Inorg. Chem.* **1973**, *12*, 1.

0020-1669/88/1327-1204$01.50/0